Water use characteristics of different pioneer shrubs at different ages in western Chinese Loess Plateau: Evidence from δ^2H offset correction

ZHANG Yu[1,2], ZHANG Mingjun[1,2*], QU Deye[1,2], WANG Shengjie[1,2], Athanassios A ARGIRIOU[3], WANG Jiaxin[1,2], YANG Ye[1,2]

[1] College of Geography and Environmental Science, Northwest Normal University, Lanzhou 730070, China;
[2] Key Laboratory of Resource Environment and Sustainable Development of Oasis, Gansu Province, Northwest Normal University, Lanzhou 730070, China;
[3] Laboratory of Atmospheric Physics, Department of Physics, University of Patras, GR-26500 Patras, Greece

Abstract: *Caragana korshinskii* Kom. and *Tamarix ramosissima* Ledeb. are pioneer shrubs for water and soil conservation, and for windbreak and sand fixation in arid and semi-arid areas. Understanding the water use characteristics of different pioneer shrubs at different ages is of great importance for their survival when extreme rainfall occurs. In recent years, the stable isotope tracing technique has been used in exploring the water use strategies of plants. However, the widespread δ^2H offsets of stem water from its potential sources result in conflicting interpretations of water utilization of plants in arid and semi-arid areas. In this study, we used three sets of hydrogen and oxygen stable isotope data (δ^2H and $\delta^{18}O$, corrected $\delta^2H_{\_c1}$ based on SW-excess and $\delta^{18}O$, and corrected $\delta^2H_{\_c2}$ based on −8.1‰ and $\delta^{18}O$) as inputs for the MixSIAR model to explore the water use characteristics of *C. korshinskii* and *T. ramosissima* at different ages and in response to rainfall. The results showed that $\delta^2H_{\_c1}$ and $\delta^{18}O$ have the best performance, and the contribution rate of deep soil water was underestimated because of δ^2H offset. During the dry periods, *C. korshinskii* and *T. ramosissima* at different ages both obtained mostly water from deeper soil layers. After rainfall, the proportions of surface (0–10 cm) and shallow (10–40 cm) soil water for *C. korshinskii* and *T. ramosissima* at different ages both increased. Nevertheless, there were different response mechanisms of these two plants for rainfall. In addition, *C. korshinskii* absorbed various potential water sources, while *T. ramosissima* only used deep water. These flexible water use characteristics of *C. korshinskii* and *T. ramosissima* might facilitate the coexistence of plants once extreme rainfall occurs. Thus, reasonable allocation of different plants may be a good vegetation restoration program in western Chinese Loess Plateau.

Keywords: stable isotope; *Caragana korshinskii*; *Tamarix ramosissima*; water uptake pattern; isotope depletion

Citation: ZHANG Yu, ZHANG Mingjun, QU Deye, WANG Shengjie, Athanassios A ARGIRIOU, WANG Jiaxin, YANG Ye. 2022. Water use characteristics of different pioneer shrubs at different ages in western Chinese Loess Plateau: Evidence from δ^2H offset correction. Journal of Arid Land, 14(6): 653–672. https://doi.org/10.1007/s40333-022-0018-8

1 Introduction

Water is an important factor for vegetation growth, which determines the ecosystem functions in arid and semi-arid areas (Porporato et al., 2004; Wang et al., 2017). It restricts vegetation coverage, species richness, vegetation growth, biomass, and diversity in ecologically vulnerable

*Corresponding author: ZHANG Mingjun (E-mail: mjzhang2004@163.com)
Received 2022-03-11; revised 2022-05-30; accepted 2022-06-01

areas (Bai et al., 2004; Chang et al., 2019; Gao et al., 2011; Heras et al., 2011). It also influences the sustainability of the reestablishment of vegetation in water-scarce areas (Jia et al., 2012; Yang et al., 2014; Huo et al., 2018). Plants satisfy their water needs from deeper soil water and groundwater during the dry season, while they uptake water from shallow soil layers during the wet season (Dawson and Pate, 1996; Asbjornsen et al., 2008; Wang et al., 2017). In addition, plants with dimorphic root systems can absorb water from both shallow and deep soil layers (Dawson and Pate, 1996; Nie et al., 2011; Yang et al., 2015). These flexible water use characteristics reflect ecological plasticity, and are very beneficial to the growth, reproduction, and competition of plants (Eggemeyer et al., 2009; Moreno-Gutiérrez et al., 2012). Thus, water use characteristics of different plants play a significant role in understanding the interspecies competition and simulating the hydrological process at the soil–plant–atmosphere continuum (Sprenger et al., 2016; Chen et al., 2017; Vargas et al., 2017).

Stable isotopes of hydrogen and oxygen have been widely used in determining plant water sources (Rothfuss and Javaux, 2017; Wang et al., 2017; Allen et al., 2019; Chen et al., 2021) based on the assumption that no isotopic fraction occurs during root water uptake (Dawson and Ehleringer, 1991). The isotopic ratios of plant xylem water can be regarded as the weighted average of potential water sources and their contribution rates (Ehleringer and Dawson, 1992). However, Lin and Sternberg (1993) found that the δ^2H of vacuum-extracted xylem water from mangroves was more depleted than that of source water. The reason can be attributed to the hydrogen isotope fractionation during the suction of water by the plant. Ellsworth and Williams (2007) studied sixteen xerophytic and semi-xerophytic trees and shrubs under controlled conditions, and found a 3‰–9‰ depletion in the δ^2H of plant xylem water. This hydrogen isotope depletion is not just a special case, but also has been found in other tree species, including semi-arid shrub species (Wang et al., 2017), coniferous and broadleaf forests (Brooks et al., 2010; Bowling et al., 2017; Geris et al., 2017; Barbeta et al., 2019; Goldsmith et al., 2019), and tropical rainforests (Hannes et al., 2018; Brum et al., 2019). The isotope tracing technique has contradictory interpretations in water utilization of plants if δ^2H offsets are not considered (Barbeta et al., 2019; Barbeta et al., 2022).

Caragana korshinskii Kom. is a plant of the genus Leguminous *Caragana* with a relatively developed root system and strong adaptability. It is the preferred shrub for soil and water conservation and ecological restoration in water-scarce areas (Fang et al., 2013; Chen et al., 2021). *Tamarix ramosissima* Ledeb. is a shrub with a well-developed root system, which is drought-tolerant and salt-alkali-resistant. It plays an important role in wind prevention, which is used for sand fixation and ecological restoration on the Chinese Loess Plateau (Li et al., 2015). On the Loess Plateau, the groundwater is buried too deeply to be a source of water for vegetation, and plants can only survive on soil moisture replenished by rainfall (Wang et al., 2017; Chen et al., 2021). However, the climate of northwestern China has undergone a transition from warm-drying to warm-wetting in recent years (Yao et al., 2020; Zhang et al., 2021), which has inevitably lead to variations in plant water use patterns. Thus, whether these two pioneer shrubs can adequately adjust water use characteristics in response to highly variable rainfall patterns is crucial for their survival. Previous research has shown that *T. ramosissima* mainly uses deep soil water (Zhou et al., 2017; Su et al., 2020), and *C. korshinskii* exhibits significantly seasonal patterns in water source uptake (Gao et al., 2018; Zhang et al., 2020). However, these researches did not consider δ^2H offsets of plant xylem water. Barbeta et al. (2019) found that monoisotopic tracers are insufficient to be identified as plant water sources when the stem water isotopic composition is matched to multiple water sources. Therefore, it is necessary to correct the δ^2H offsets when quantifying sources of root water absorption (Li et al., 2021). Thus, this paper researched the water use characteristics of *C. korshinskii* and *T. ramosissima* at different ages after rainfall in the Chinese Loess Plateau based on corrected isotope data. The objectives of this study were to: (1) analyze the performance of these three sets of data (δ^2H and $\delta^{18}O$, corrected $\delta^2H_{\_c1}$ based on SW-excess and $\delta^{18}O$, and corrected $\delta^2H_{\_c2}$ based on −8.1‰ and $\delta^{18}O$) input into the MixSIAR model; and (2) investigate the water use characteristics of *C. korshinskii* and *T. ramosissima* at

different ages after rainfall and their responses.

2 Materials and methods

2.1 Study area

This study was conducted in the western Chinese Loess Plateau, Lanzhou City, Gansu Province (36°07′N, 103°44′E; Fig. 1). The study area has a mid-temperate continental climate with mean annual precipitation ranging from 270 to 320 mm. The precipitation is unevenly distributed throughout the year (mainly from June to September). The annual mean air temperature is 10.0 ℃, with a minimum value of –9.0 ℃ in January and the highest value of 29.9 ℃ in July. The terrain is higher in the north and lower in the south, the altitude ranges between 1560 and 2067 m a.s.l., and the slope is generally steeper than 30 ° (Wu et al., 2006). The soil is mainly light sierozem, with a pH value of 8.0–9.0. The vegetation coverage is low, mainly consisting of shrubs such as *Tamarix ramosissima*, *Caragana korshinskii* and *Reaumuria soongorica* (Pall.) Maxim., and herbs such as *Agropyron cristatum* (L.) Gaertn. and *Peganum multisectum* (Maxiam.) Bobr. (Zhang et al., 2020).

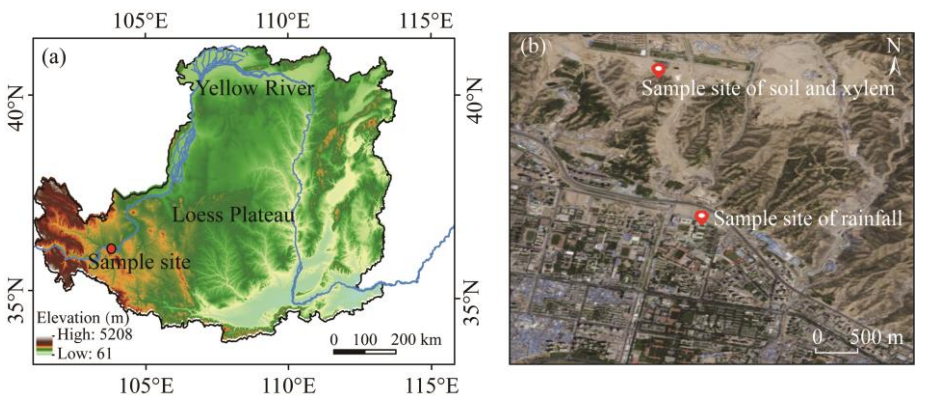

Fig. 1 Sample location on the western Chinese Loess Plateau (a) and sample sites of soil, xylem, and rainfall (b)

2.2 Experimental design and sample collection

The twig xylem of juvenile, intermediate, and adult *C. korshinskii* and *T. ramosissima* were sampled from July to October 2020 (Table 1). Sampling were conducted on days 1, 3, and 5 after rainfall events on 17–18 July (12.9 mm) and 23 August (15.0 mm). Each sampling was performed between 08:00 and 10:00 (LST). Three replicate samples were taken from the shrubs. Twig xylem samples were cut-off from well-grown plants; and the length of each sample ranged between 3 and 5 cm, and its diameter was approximately 0.5 cm. The bark was quickly removed to retain only the xylem, placed into a glass bottle with screw caps, sealed with parafilm, and kept frozen in a refrigerator (–20 ℃). Simultaneously, we excavated a soil core at a depth of 200 cm near the sampled shrubs, and soil samples were taken at depths of 5, 10, 15, 20, 30, 40, 50, 60, 70, 80, 90, 100, 120, 140, 160, 180, and 200 cm, with two replicates per individual. Each soil sample was divided into two parts: one part was placed into glass vials, sealed with parafilm, and stored in a refrigerator (–20 ℃) until isotopic analysis, and the other was used to measure its gravimetric water content (SWC, %) by drying it at 105 ℃ for 24 h. The rainfall samples in 2020 were collected from a rain collector comprised of a polyethylene tank and a funnel fitted with a ping-pong ball, which was set in the meteorological field of the New Campus of Northwest Normal University, China, at approximately 2.5 km from the soil and xylem sample site. The temperature and precipitation data in 2020 were collected from the nearest Gaolan station (China Meteorological Data Service Centre) to the study site.

Table 1 Morphological traits of *C. korshinskii* and *T. ramosissima* at different ages

Plant	Planting year (a)	Height (m)	Crown width (m)
Juvenile *C. korshinskii*	2	0.7	0.9
Intermediate *C. korshinskii*	4	1.0	1.4
Adult *C. korshinskii*	8	1.8	3.0
Juvenile *T. ramosissima*	6	2.2	1.5
Intermediate *T. ramosissima*	15	3.0	2.6
Adult *T. ramosissima*	24	4.0	5.0

2.3 Isotopic analyses

All xylem and soil water samples were extracted using an automatic cryogenic extraction system (LI-2200, BJJL, Beijing, China) in the Stable Isotope Laboratory, College of Geography and Environmental Science, Northwest Normal University, China. The vacuum threshold was controlled below 1 Pa/s, the heating temperature was 105 ℃, and the extraction time was 3 h. We randomly selected portion of those samples, weighed them after the extraction, and dried them at 105 ℃ for 24 h to ensure that the extraction efficiency exceeded 98% (Yang et al., 2015).

The isotopic compositions of the extracted soil water, xylem water, and rainfall samples were measured using an isotopic ratio infrared spectroscopy (IRIS) system (T-LWIA-45-EP, ABB-Los Gatos Research, CA, USA). The analytical accuracies were ±1‰ for δ^2H and ±0.3‰ for $\delta^{18}O$. The composition of δ^2H and $\delta^{18}O$ is expressed in per mil relative to the Vienna Standard Mean Ocean Water (VSMOW):

$$\delta = \left(\frac{R_{\text{sample}}}{R_{\text{standard}}} - 1 \right) \times 1000‰ , \quad (1)$$

where R_{sample} and R_{standard} are the ratios of $^2H/^1H$ or $^{18}O/^{16}O$ of the sample and the standard (VSMOW), respectively.

Organic contaminants (such as methanol, ethanol, and other biological volatile substances) in the water extracted from the twig xylem and soil used cryogenic vacuum distillation would affect the isotopic measurements by the IRIS method (Martín-Gómez et al., 2017). Therefore, we used the spectral analysis software of Los Gatos Research (ABB-Los Gatos Research, CA, USA) to correct the soil and twig xylem water isotope data based on the index of the measured absorption spectrum to eliminate organic contaminants (Schultz et al., 2011; Leen et al., 2012).

2.4 Data analysis

Landwehr and Coplen (2006) proposed the line-conditioned excess (lc-excess) to evaluate whether there is a δ^2H offset between soil water (river water and groundwater) and precipitation:

$$\text{lc-excess} = \delta^2H - a\delta^{18}O - b , \quad (2)$$

where a and b are the slope and intercept of local meteoric water line (LMWL), respectively. The lc-excess describes the non-equilibrium dynamic fractionation caused by evaporation (Landwehr et al., 2014). The average value of lc-excess of precepitation is 0‰. The lc-excess for other water bodies (e.g., soil water and river water) affected by evaporation, is usually less than 0‰. However, since the water inside a plant is more likely to originate from soil water than directly from precipitation, Barbeta et al (2019) revised Equation 2 and proposed SW-excess to describe the deviation of plant xylem water concerning soil water line (SWL):

$$\text{SW-excess} = \delta^2H - a_s\delta^{18}O - b_s , \quad (3)$$

where a_s and b_s are the slope and intercept of SWL at the same sampling point in a given period, respectively. Positive SW-excess indicates that plant xylem samples are more enriched in δ^2H than SWL, and vice-versa.

The corrected hydrogen isotope of xylem water ($\delta^2H_{\_c1}$) is:

$$\delta^2H_{\_c1} = \delta^2H - \text{SW-excess}\,. \tag{4}$$

In addition, Chen et al (2020) found that plant xylem water cryogenic extraction bias that could originate from a dynamic exchange between organic combination deuterium was the key to explaining the hydrogen isotope depletion. They proposed a stem water hydrogen isotope correction method based on the stem relative water content:

$$\delta^2H_{\_c2} = \delta^2H - \varepsilon/S\,, \tag{5}$$

where $\delta^2H_{\_c2}$ is the corrected hydrogen isotope of stem water; ε is the deuterium offset between cryogenically extracted stem water and true xylem water, which is the regression function of the relative water content of the stem; and S is the measurement uncertainty (Evaristo et al., 2015):

$$S = [(\delta^2H_{\text{analytical error}})^2 + (\delta^{18}O_{\text{analytical error}})^2]^{0.5}\,. \tag{6}$$

Since we did not measure the stem relative water content, we treated ε as a fixed value of –8.1‰, which corresponds to the species-averaged value for the offset of $\delta^2H_{\text{stem\_CVD}}$ (the hydrogen isotope ratio of water cryogenically extracted from plant stem samples) from δ^2H_{xylem} (δ^2H of plant source water) as obtained from the study of Chen et al. (2020).

At present, there are mainly methods such as the graphical inference method, two-source or three-source linear mixing models, multiple linear mixing model (IsoSource), Bayesian mixing models (MixSIR, SIAR, and MixSIAR), and other methods based on the stable isotopes to trace water sources of plants. Among them, MixSIAR not only considered the uncertainty of root water absorption but also provided an optimal solution rather than a series of feasible solutions (Stock and Semmens, 2013; Rothfuss and Javaux, 2017; Antunes et al., 2018; Wang et al., 2019). Therefore, the Bayesian mixing model MixSIAR was used to estimate the contribution of different potential water sources to the plants. Since isotope fractionation does not occur during root water uptake, the discriminant value was set to 0 (Brunel et al., 1995; Oerter et al., 2019). The run length of the Markov Chain Monte Carlo (MCMC) was set to 'long' (chain length=300,000; burn-in=200,000; thin=100; and chains=3) to ensure that the model converged, which was tested by applying the Gelman–Rubin and the Geweke diagnostic. The mean value was presented as the output of the MixSIAR. To evaluate the effect of δ^2H offset in xylem water on quantifying root uptake water, we used three sets of data: δ^2H and $\delta^{18}O$, corrected $\delta^2H_{\_c1}$ based on SW-excess and $\delta^{18}O$, and corrected $\delta^2H_{\_c2}$ based on –8.1‰ together with the $\delta^{18}O$ input MixSIAR model. The performance of three sets of data was assessed by the Akaike information criterion (AIC), Bayesian information criterion (BIC), and root mean square error (RMSE). The input dataset with the smallest AIC, BIC, and RMSE values was the best type.

$$\text{RMSE} = \sqrt{\left[\frac{1}{n}\sum_{i=1}^{n}(p_i - o_i)^2\right]}\,, \tag{7}$$

where n is the number of validation samples; and p_i and o_i are the predicted and observed values of xylem water isotope values, respectively.

$$p_i = \sum_{j=1}^{k} f_i \delta_A\,, \tag{8}$$

where j is the j^{th} water source used by plants; k is the number of water sources (k=4 in this study); f is the proportion of water sources calculated by the MixSIAR model; and δ_A is the isotopic composition of the water sources.

One-way analysis of variance (ANOVA) with the least significant difference (LSD) method (P<0.05) was used to examine isotope differences of different water bodies; if P≥0.05, it was considered that there was no difference. In addition, the relationship between the contribution rate of potential soil water sources and environmental factors was analyzed using Pearson's correlation coefficient test. We divided the whole sampling profile into four potential soil water sources based on the variability in δ^2H, $\delta^{18}O$, and SWC, i.e., surface (0–10 cm), shallow (10–40 cm), middle (40–100 cm), and deep (100–160 cm) soil water.

3 Results

3.1 Soil water content

The vertical distribution of soil water content for *C. korshinskii* and *T. ramosissima* at different ages is shown in Figure 2. The 0–40 cm soil layers of *C. korshinskii* and *T. ramosissima* at different ages were found to have relatively higher soil water contents, and the temporal variation of soil water content after rainfall events in the 0–40 cm was more obvious than that in the 40–100 cm, suggesting 0–40 cm soil layers are more susceptible to rainfall infiltration and evaporation. In addition, the 40–100 cm soil water content had relatively small seasonal differences with gentle fluctuation, and the soil water content below 100 cm was the lowest with smooth and low fluctuation. The soil water content of the whole profile was the smallest before rainfall (9 July and 16 August), then increased rapidly at 1 d after rainfall (19 July and 24 August), and gradually decreased over time.

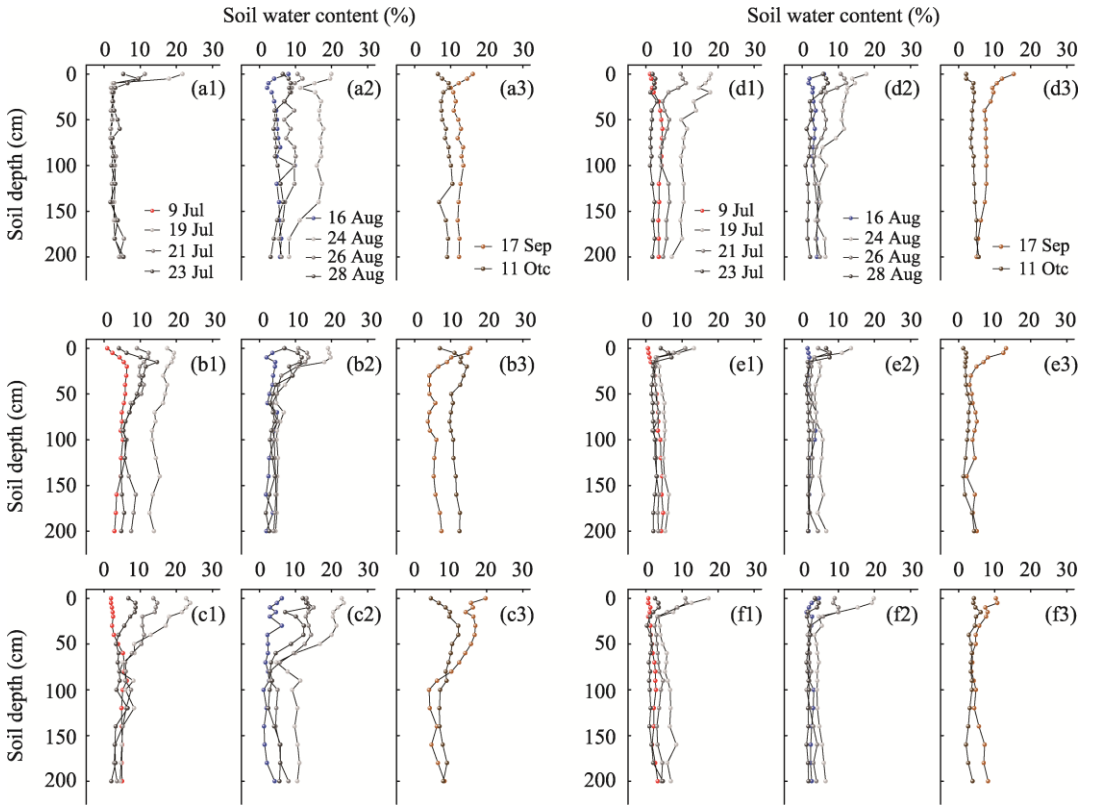

Fig. 2 Variations in the soil water content of juvenile *C. korshinskii* (a1–a3), intermediate *C. korshinskii* (b1–b3), adult *C. korshinskii* (c1–c3), juvenile *T. ramosissima* (d1–d3), intermediate *T. ramosissima* (e1–e3), and adult *T. ramosissima* (f1–f3)

3.2 Isotopic composition of different water bodies

The $\delta^{18}O$ of precipitation ranged from –18.06‰ to 1.58‰, and the annual precipitation weighted average values were –8.21‰. The $\delta^{2}H$ ranged from –126.82‰ to –28.73‰, with the annually weighted average value of –49.91‰. The maximum value of the weighted monthly precipitation was observed in June ($\delta^{2}H$ and $\delta^{18}O$ being –12.16‰ and –2.91‰, respectively), and the minimum value was observed in January (–96.41‰ for $\delta^{2}H$ and –13.72‰ for $\delta^{18}O$) (Fig. S1). The LMWL is $\delta^{2}H=6.95(\pm0.26)\delta^{18}O+3.25(\pm2.31)$, $R^{2}=0.95$, and $P<0.01$; its slope and intercept were less than those of the GMWL (Craig, 1961), suggesting the climatic characteristics of intense evaporation in arid and semi-arid areas (Fig. 3).

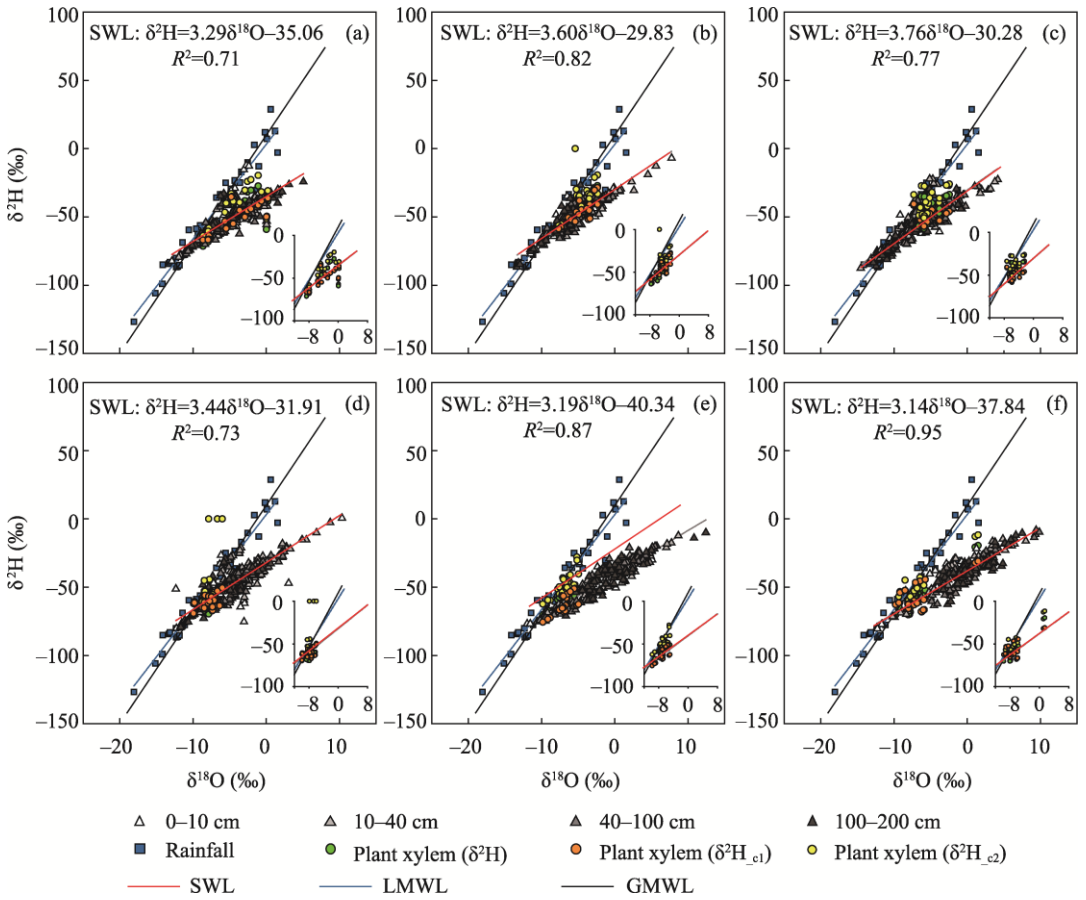

Fig. 3 Relationships between δ^2H and $\delta^{18}O$ of rainfall, soil water, and plant xylem water for juvenile *C. korshinskii* (a), intermediate *C. korshinskii* (b), adult *C. korshinskii* (c), juvenile *T. ramosissima* (d), intermediate *T. ramosissima* (e), and adult *T. ramosissima* (f). SWL is the soil water line based on soil water isotope values, and LMWL is the local meteoric water line. GMWL ($\delta^2H=8\delta^{18}O+10$) is plotted for reference. Insets show the linear regression relationship between δ^2H (δ^2H, δ^2H_{c1}, and δ^2H_{c2}) and $\delta^{18}O$ in plant xylem water.

Hydrogen and oxygen isotopes in soil water showed similar vertical distributions and temporal changes; thus, we used $\delta^{18}O$ to analyze the characteristics of soil water isotopic compositions (Figs. S2 and S3). The $\delta^{18}O$ of soil water varied with soil depth and plant species (Fig. S3; Table S1). The $\delta^{18}O$ of the 0–40 cm soil water exhibited greater temporal variability than that of the 40–100 cm soil water, and then stabilized with increasing of soil depths. In addition, the soil water $\delta^{18}O$ of the two shrubs at different ages showed obvious differences ($P<0.05$). The $\delta^{18}O$ values of soil water were –4.69‰ (±3.39‰) for juvenile *C. korshinskii*, –5.27‰ (±3.14‰) for intermediate *C. korshinskii*, –7.01‰ (±3.47‰) for adult *C. korshinskii*, –4.27‰ (±3.61‰) for juvenile *T. ramosissima*, –1.06‰ (±4.38‰) for intermediate *T. ramosissima*, and −0.38‰ (±3.80‰) for adult *T. ramosissima*. Prior to rainfall (9 July and 16 August), the $\delta^{18}O$ was the most enriched, then decreased rapidly at 1 d after rainfall (19 July and 24 August), and gradually increased over time (Fig. S3). The relationships between δ^2H and $\delta^{18}O$ in soil water for juvenile, intermediate, and adult *C. korshinskii* and *T. ramosissima* are shown in Figure 3. The slope of the soil water lines (SWL) increased with age for *C. korshinskii*, while the inverse trend was observed for *T. ramosissima*. All the SWLs were plotted on the lower right of the LMWL and intersected with it, indicating that soil water originated from rainfall and was affected by different degrees of evaporation.

Significant differences in xylem water isotope values between different species were observed ($P<0.05$), indicating that *C. korshinskii* and *T. ramosissima* may have distinct water use

characteristics. Significant differences were observed in the xylem water isotopes of *C. korshinskii* at different ages (P<0.05), while *T. ramosissima* did not present such a discrepancy with age (P≥0.05). The isotopic composition of *C. korshinskii* and *T. ramosissima* at different ages was found to be near that of soil water, suggesting that the plants obtain water primarily from soil horizons (Fig. 3). After the rainfall events of 17–18 July and 23 August, there was no significant variation in the isotopic composition of plant xylem water (Table S1), which was attributed to the fact that the isotope signal of rainfall needed a certain time to transport to xylem of plants.

3.3 δ^2H offset of xylem water

The δ^2H offset between xylem water and SWL was calculated by SW-excess. The average SW-excess values were 2.43‰, 0.42‰, and 3.48‰ for juvenile, intermediate, and adult *C. korshinskii*, respectively, while the average SW-excess values were –1.03‰, 3.16‰, and 1.85‰ for juvenile, intermediate, and adult *T. ramosissima*, respectively (Fig. 4). This finding was distinct from that of previous studies. The SW-excess has positive and negative values, which may be related to the occurrence of rainfall events. The average SW-excess after rainfall on 17–18 July (SW-excess>0) was larger than that on 23 August (SW-excess<0), which was attributed to the slope of SWL after rainfall on 17–18 July being less than that on 23 August (except for intermediate *T. ramosissima*) (Fig. S4). It all boils down to the significantly different rainfall isotopic compositions on 17–18 July (δ^2H= –33.26‰, $\delta^{18}O$= –5.64‰) and 23 August (δ^2H= –68.76‰, $\delta^{18}O$= –11.43‰). Compared with the uncorrected δ^2H, the corrected δ^2H_{c1} and δ^2H_{c2} values from both methods were closer to the range of potential water sources (Fig. 3), indicating that these two correction methods were reasonable.

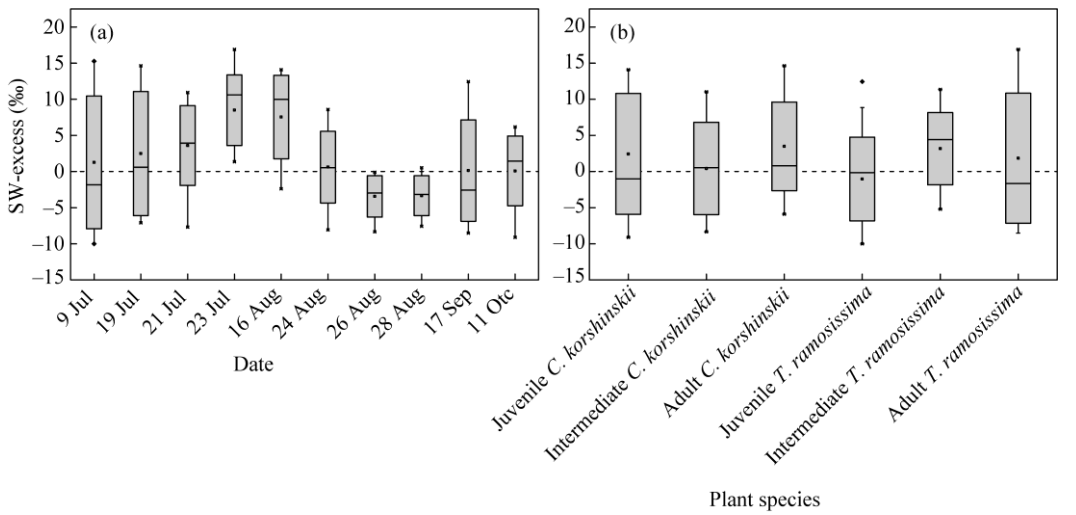

Fig. 4 Temporal variation (a) and plant species difference (b) in SW-excess. The extents of the boxes show the 25th and 75th percentiles, whiskers show the range within 1.5IQR (interquartile range), and the black rhombus denote the outliers.

3.4 Water source apportionment by three input datasets

When the isotopic compositions of potential water sources were similar, it is not sufficient to use a single isotope to analyse the water use strategies of plants to distinguish the contribution rates of different water sources. Thus, we used three sets of isotopic datasets as inputs to the MixSIAR model: δ^2H and $\delta^{18}O$, δ^2H_{c1} and $\delta^{18}O$, and δ^2H_{c2} and $\delta^{18}O$, and the obtained results were different (Figs. 5 and 6). The AIC, BIC, and RMSE values showed that the δ^2H_{c1} and $\delta^{18}O$ pairs are the best performing types in identifying water use characteristics (Table 2). In contrast, the performance of δ^2H_{c2} and $\delta^{18}O$ was not better than that of δ^2H and $\delta^{18}O$ because we did not

directly measure the water content of the plant stems but used the constant ε of –8.1‰. This result also showed that the value of –8.1‰ for δ^2H bias cannot be used as a general correction factor. Moreover, the contribution of deep soil water was underestimated because of hydrogen isotope offset (Table S2). Therefore, the $\delta^2H_{\_c1}$ and $\delta^{18}O$ datasets were used to analyse the root water uptake patterns of pioneer shrubs of different ages.

Table 2 Performance of water source contribution using three input datasets to the MixSIAR model

Input dataset	AIC	BIC	RMSE
δ^2H and $\delta^{18}O$	287.56	291.71	14.28
$\delta^2H_{\_c1}$ and $\delta^{18}O$	267.25	271.40	13.22
$\delta^2H_{\_c2}$ and $\delta^{18}O$	289.00	293.16	13.74

Note: AIC, Akaike information criterion; BIC, Bayesian information criterion; RMSE, root mean square error.

The relative proportions of soil water sources to *C. korshinskii* at different ages after rainfall calculated by the MixSIAR model with three input datasets are shown in Figure 5. On 9 July, intermediate and adult *C. korshinskii* obtained most of their water from the 100–200 cm soil layers, which was due to the higher soil water content in the 100–200 cm layers (no sampling for juvenile *C. korshinskii*). Juvenile *C. korshinskii* absorbed water from all four soil water layers at 1 d after rainfall on 17–18 July, and shifted to both use the 10–40 and 40–100 cm soil water at 3 and 5 d after rainfall. On 16 August, juvenile *C. korshinskii* tended to extract the 10–40 and 40–100 cm soil water, shifted to use the 0–10 cm soil water at 3 and 5 d after rainfall on 23 August, and the proportions of the 0–10 cm gradually increased over time. Juvenile *C. korshinskii* mainly utilized the 0–10 and 10–40 cm soil water during the late growing season (September and October), and the proportions gradually increased. Intermediate *C. korshinskii* tended to extract the 0–40 cm soil water at 1 d after rainfall on 17–18 July, and the proportional contributions of the 0–40 cm soil water gradually decreased at 3 and 5 d after rainfall. On 16 August, intermediate *C. korshinskii* obtained water mostly from the 0–10 cm soil water, used the 10–40 cm soil water at 1 d after rainfall on 23 August, and then shifted to use the 0–10 cm soil water at 3 and 5 d after rainfall. Intermediate *C. korshinskii* mainly utilized the 0–10 and 10–40 cm soil water during the late growing season (September and October), and the proportions gradually decreased. Adult *C. korshinskii* obtained water from the 40–100 cm soil water at 1 d after rainfall on 17–18 July and then gradually increased the proportions of the 0–40 cm soil water at 5 d after rainfall. On 16 August, adult *C. korshinskii* utilized water mostly from the 0–10 cm soil water and used the 0–10 cm (50.7% (±3.7%)) and 100–200 cm (43.1% (±2.1%)) soil water at 1 d after rainfall on 23 August, and the proportions of the 0–40 cm soil water steadily increased over time. Adult *C. korshinskii* mainly absorbed the 0–10 and 10–40 cm soil water during the late growing season (September and October), and gradually increased the proportional contributions.

Figure 6 shows the relative proportions of water sources to *T. ramosissima* of various ages after rainfall, as calculated by the MixSIAR model using three sets of input data. On 9 July, juvenile and intermediate *T. ramosissima* mainly utilized the 100–200 cm soil water, while adult *T. ramosissima* absorbed the water from the 40–100 and 100–200 cm soil layers. On 17–18 July, a rainfall of 12.9 mm occurred. At 1 d after rainfall, juvenile *T. ramosissima* mainly used the 0–10 and 100–200 cm soil water and shifted to the 100–200 cm soil water at 3 and 5 d after rainfall. The contribution of the 0–10 cm soil water for intermediate *T. ramosissima* was relatively larger (>70%) at 1 d after rainfall, and the proportion of the 10–40 cm soil water gradually increased at 3 and 5 d after rainfall. On the first day after rainfall, the proportional contributions of the 0–10 cm soil water for adult *T. ramosissima* were larger (more than 70%) than those of the other soil layers, and this proportion dramatically increased to a proportion of 98% at 3 d after rainfall. However, the water source for adult *T. ramosissima* shifted from the 0–10 cm at 3 d to the 100–200 cm soil water at 5 d after rainfall. On 16 August, juvenile and adult *T. ramosissima* extracted the 40–100 cm soil layer as the main water source, while intermediate *T. ramosissima* used water from the 10–40 cm soil layer. On the first day after rainfall on 23 August (15.0 mm),

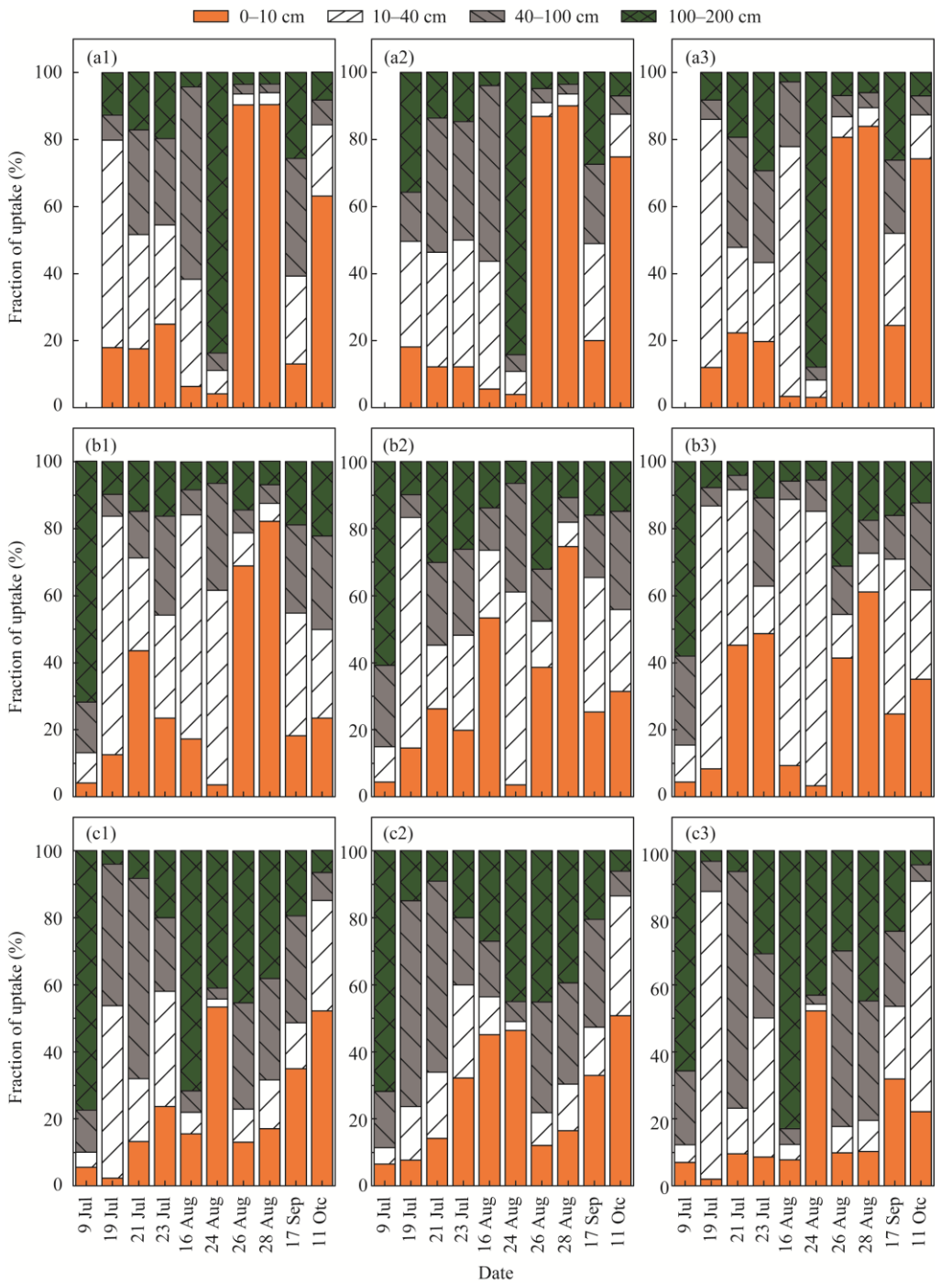

Fig. 5 Relative proportions of water sources used by juvenile *C. korshinskii* (a1–a3), intermediate *C. korshinskii* (b1–b3), and adult *C. korshinskii* (c1–c3) with the MixSIAR model based on δ^2H and $\delta^{18}O$, $\delta^2H_{\_c1}$ and $\delta^{18}O$, and $\delta^2H_{\_c2}$ and $\delta^{18}O$

the proportional contributions of soil water in each soil layer for juvenile *T. ramosissima* were approximate, and the 0–10 cm (90%) soil water was used at 3 d after rainfall. Besides, the contribution of the 0–10 and 10–40 cm soil layers for juvenile *T. ramosissima* was even higher at 5 d. Intermediate *T. ramosissima* mainly utilized the 0–10 and the 10–40 cm soil water at 1 d after rainfall, switched to using the 10–40 and 100–200 cm soil water at 3 d, and the 10–40 cm (70%)

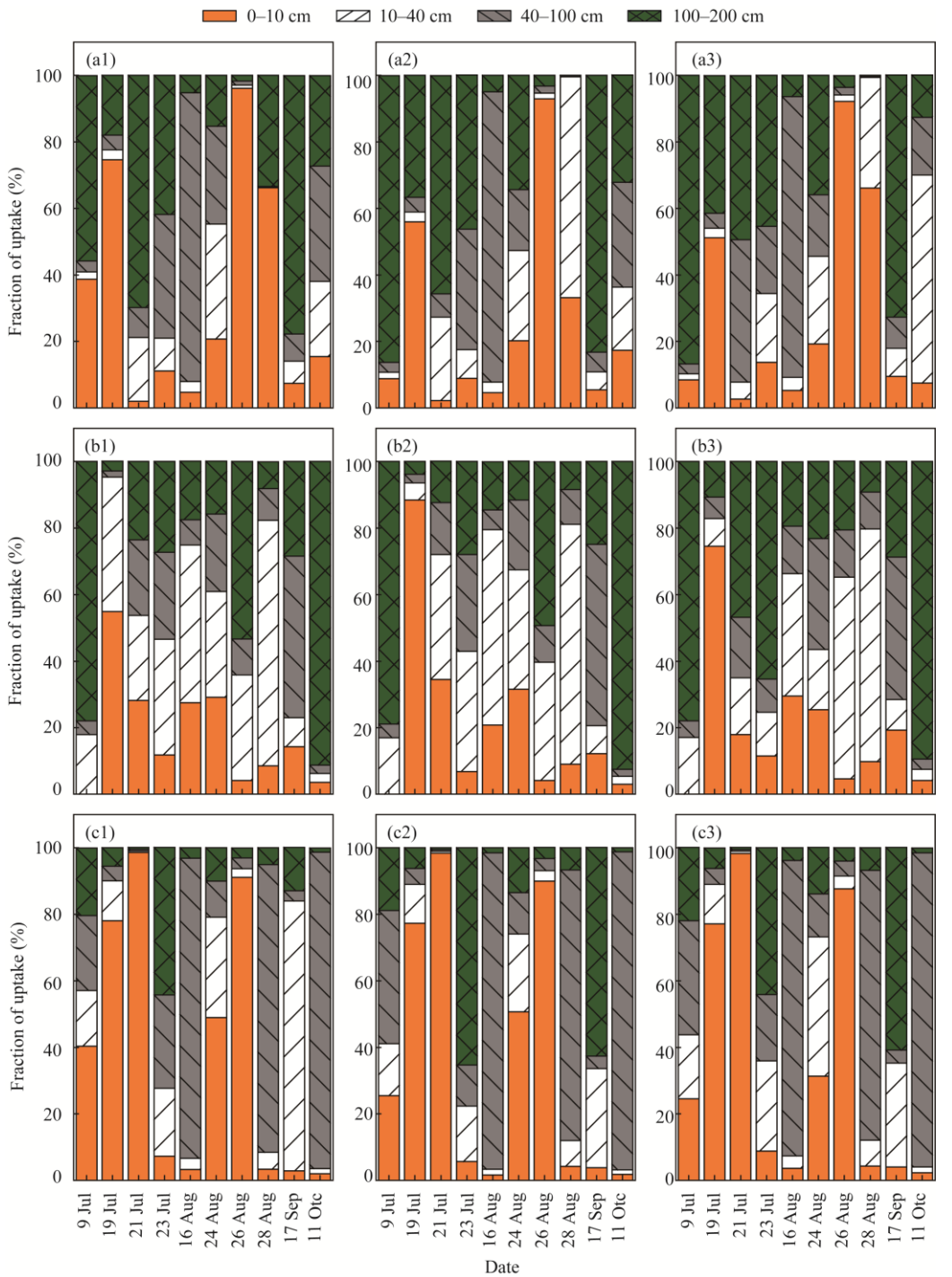

Fig. 6 Relative proportions of water sources used by juvenile *T. ramosissima* (a1–a3), intermediate *T. ramosissima* (b1–b3), and adult *T. ramosissima* (c1–c3) with the MixSIAR model based on δ^2H and $\delta^{18}O$, δ^2H_{c1} and $\delta^{18}O$, and δ^2H_{c2} and $\delta^{18}O$

soil water at 5 d, respectively. Adult *T. ramosissima* mainly absorbed the 0–10 and 10–40 cm soil water at 1 d after rainfall and shifted to utilize the 0–10 cm soil water at 3 d and 40–100 cm soil layer water (70%) at 5 d, respectively. In September, 100–200 cm soil water was the primary water source for juvenile and adult *T. ramosissima*, while intermediate *T. ramosissima* utilized the water in the 40–100 cm soil layer. In October, the proportions of the 40–100 and 100–200 cm,

100–200 cm (90%), and 40–100 cm (90%) soil water were higher for juvenile, intermediate, and adult *T. ramosissima*, respectively.

4 Discussion

4.1 Variation in stable isotopes of soil water after rainfall

In the Loess Plateau, the groundwater is buried too deeply to be a source of water for plants, and plants can only survive on soil moisture originally derived from rainfall (Wang et al., 2017). In this study, the temporal variation of soil water and isotopic compositions of the 0–40 cm varied dramatically after rainfall than that of deeper soil layers (Figs. 2, S2, and S3), suggesting that the 0–40 cm soil water was more susceptible to rainfall and evaporation (Rossatto et al., 2012). This was consistent with the findings of Sprenger et al. (2017), who proposed subsequent fading of the fractionation effect: the stable isotope in the upper soil water varied dramatically as soon as rainfall infiltrated into the soil, and became weaker with depth. Before rainfall (9 July and 16 August), the isotope values of soil water were most enriched and then decreased dramatically at 1 d after rainfall (19 July and 24 August) because of the infiltration of rainfall with a negative isotopic composition. The isotopic compositions of soil water gradually increased at 3 and 5 d after rainfall due to the stronger evaporation effects (Dai et al., 2015).

4.2 Water uptake patterns of *C. korshinskii* and *T. ramosissima* at different ages

C. korshinskii gradually increased the proportion of deeper (100–200 cm) soil water with age. Juvenile and intermediate *C. korshinskii* mainly utilized the water from the 0–10 and 10–40 cm soil layers, while adult *C. korshinskii* mainly absorbed water from the 40–100 and 100–200 cm soil layers. In this study, during the dry period (9 July), intermediate and adult *C. korshinskii* obtained water mostly from deeper (100–200 cm) soil water (no sampling for juvenile *C. korshinskii*). *C. korshinskii* at different ages switched their sources from different soil layers after rainfall (Figs. 5 and 6), and the response of water use characteristics of *C. korshinskii* at different ages to rainfall varied (Tables S3 and S4). When antecedent soil water was deficient, the water uptake patterns of juvenile *C. korshinskii* after rainfall tended to be more homogeneous in different soil horizons (after rainfall on 17–18 July). However, when antecedent soil water was sufficient, juvenile *C. korshinskii* water use patterns were more sensitive to rainfall, and the main water sources after rainfall shifted from the 100–200 to the 0–10 cm of soil water (after rainfall on 23 August). This result is in line with the result of Dai et al. (2015), who found that the water use strategies of *Haloxylon ammodendron* (C. A. Mey.) Bunge were more sensitive to rainfall in spring with abundant surface soil water than in dry summer. The water use strategies of intermediate *C. korshinskii* can respond to rainfall immediately, and plants tended to utilize the 0–40 cm soil water after rainfall on 17–18 July and 23 August. Adult *C. korshinskii* had delayed responses to water use after rainfall, and the contribution of the 0–40 cm soil water generally increased gradually at 1, 3, and 5 d after rainfall.

T. ramosissima is a deep root plant, and plant roots distributed in surface soil mainly absorbed soil moisture provided by rainfall, while deeper roots absorbed soil water supplied by winter and spring precipitation or groundwater in drought environments (Williams and Ehleringer, 2000; Chimner and Cooper, 2004; Su et al., 2020). The roots in the surface soil may be dormant under drought conditions, and are reactivated by rainfall. Therefore, plants only rely on their deep roots to utilize water from the soil when there is less rainfall and low shallow soil water content (Ehleringer and Dawson, 1992). When the rainfall amount reaches a certain threshold, the shallow soil water content increases, and plant roots begin to form and maintain the function of absorbing surface soil moisture (Duan et al., 2008), which helps to reduce energy consumption as demonstrated in previous studies (Ogle and Reynolds, 2004; Schenk, 2008; Sun et al., 2011). In this study, during the dry period (July 9), juvenile and intermediate *T. ramosissima* absorbed deeper (100–200 cm) soil water, while adult *T. ramosissima* mainly utilized water from middle (40–100 cm) and deep (100–200 cm) soil layers. After rainfall, *T. ramosissima* of different ages

tended to absorb surface (0–10 cm) and shallow (10–40 cm) soil water supplied by rainfall, which was the same as the result of Cui et al. (2015) in the Gobi area of Dunhuang, China. The response of the water use characteristics of *T. ramosissima* at different ages to rainfall varied (Tables. S3 and S4). Water use strategies of juvenile *T. ramosissima* were sensitive to rainfall when antecedent soil water was sufficient. The water use strategies of intermediate and adult *T. ramosissima* can both respond to rainfall immediately. Intermediate *T. ramosissima* tended to utilize the 0–40 cm soil water after rainfall on 17–18 July and 23 August, and the proportion gradually decreased. Adult *T. ramosissima* tended to absorb the 100–200 and 40–100 cm soil water at 5 d after rainfall on 17–18 July and 23 August, respectively.

The contribution rates of potential water sources for *C. korshinskii* and *T. ramosissima* at different ages were also correlated with environmental data (rainfall, vapour pressure deficit, and soil water content) (Table S5). The discrepancy in the water source contribution of *C. korshinskii* was mainly reflected in the relationship with soil water content. Nevertheless, the difference in contribution rates of *T. ramosissima* was reflected in the correlation with the cumulative rainfall 7 d before sampling, the average vapour pressure deficit 7 d before sampling, and the soil water content.

4.3 Implications

The transition of climate from warm-drying to warm-wetting and extreme precipitation with increasing frequency on the Loess Plateau will impel plants to change their water use patterns (Gao et al., 2018). During the dry period, intermediate and adult *C. korshinskii* obtained water mostly from deeper (100–200 cm) soil water and juvenile and intermediate *T. ramosissima* absorbed deeper (100–200 cm) soil water, while adult *T. ramosissima* absorbed mostly water from the middle (40–100 cm) and deeper (100–200 cm) soil layers. After rainfall, the proportions of surface (0–10 cm) and shallow (10–40 cm) soil water for *C. korshinskii* and *T. ramosissima* at different ages both steadily increased over time. However, there were different responses to rainfall. Compared with the water use strategies of the two pioneer shrubs, we found that *C. korshinskii* absorbed various potential water sources simultaneously, while *T. ramosissima* only used deep water. These significantly different water use strategies allow them to achieve a complementary utilization of resources, and promote coexistence between species, which may provide more guidance in ecological rehabilitation and insights for the selection and management of plant species during vegetation restoration on the Loess Plateau. In vegetation restoration, plants with different water use characteristics should be combined to form a good plant configuration, and compensate for the lack of water use by different species. In this study, we attempted to analyze the performance of three datasets: δ^2H and $\delta^{18}O$, corrected $\delta^2H_{\_c1}$ based on SW-excess and $\delta^{18}O$, and corrected $\delta^2H_{\_c2}$ based on −8.1‰ and $\delta^{18}O$. The performance of $\delta^2H_{\_c2}$ and $\delta^{18}O$ was not the best because we did not directly measure the water content of plant stems but used the constant ε of −8.1‰. A higher performance may be obtained if the measured stem water content is used to correct the δ^2H offset in future studies. In addition, fine roots determine plant water uptake, and further long-term studies on root biomass, characteristic changes affecting root activity, and changes in stable isotopes over time are needed.

5 Conclusions

This study used three sets of hydrogen and oxygen stable isotope data as inputs for the MixSIAR model to explore the water use strategies and responses to rainfall of *C. korshinskii* and *T. ramosissima* at different ages in western Chinese Loess Plateau. We evaluated the performance of the three sets of data input to the MixSIAR model, and found that $\delta^2H_{\_c1}$ and $\delta^{18}O$ was the best performance type. In addition, the contribution of deep soil water was underestimated because of the δ^2H offset. During the dry periods, deeper (100–200 cm) soil water was the main source for intermediate and adult *C. korshinskii*, juvenile and intermediate *T. ramosissima*, while the middle (40–100 cm) and deeper (100–200 cm) soil water was main sources for adult *T. ramosissima* (no

sampling for juvenile *C. korshinskii*). After rainfall, the proportions of surface (0–10 cm) and shallow (10–40 cm) soil water for *C. korshinskii* and *T. ramosissima* at different ages both gradually increased. Nevertheless, there were different responses to rainfall. These flexible water use characteristics of *C. korshinskii* and *T. ramosissima* might facilitate the coexistence of plants in extreme rainfall. This study will be of great significance for vegetation restoration on the Chinese Loess Plateau.

Acknowledgements

This study was funded by the National Natural Science Foundation of China (41771035, 42071047), the Foundation for Distinguished Young Scholars of Gansu Province (20JR10RA112), the Northwest Normal University (NWNU-LKZD2021-04), and the Department of Education of Gansu Province: "Innovation Star" Program of Excellent Postgraduates (2021CXZX-217).

References

Allen S T, Kirchner J W, Braun S, et al. 2019. Seasonal origins of soil water used by trees. Hydrology and Earth System Sciences, 23(2): 1199–1210.

Antunes C, Díaz-Barradas M C, Zunzunegui M, et al. 2018. Water source partitioning among plant functional types in a semi-arid dune ecosystem. Journal of Vegetation Science, 29(4): 671–683.

Asbjornsen H, Shepherd G, Helmers M, et al. 2008. Seasonal patterns in depth of water uptake under contrasting annual and perennial systems in the corn belt region of the Midwestern U.S. Plant and Soil, 308(1–2): 69–92.

Bai Y, Han X, Wu J, et al. 2004. Ecosystem stability and compensatory effects in the Inner Mongolian grassland. Nature, 431(7005): 181–184.

Barbeta A, Jones S P, Clavé L, et al. 2019. Unexplained hydrogen isotope offsets complicate the identification and quantification of tree water sources in a riparian forest. Hydrology and Earth System Sciences, 23(4): 2129–2146.

Barbeta A, Burlett R, Martín-Gómez P, et al. 2022. Evidence for distinct isotopic composition of sap and tissue water in tree stems: consequences for plant water source identification. New Phytologist, 233(3): 1121–1132.

Bowling D R, Schulze E S, Hall S J. 2017. Revisiting streamside trees that do not use stream water: can the two water worlds hypothesis and snowpack isotopic effects explain a missing water source? Ecohydrology, 10(1): e1771, doi: 10.1002/eco.1771.

Brooks J R, Barnard H R, Coulomb R, et al. 2010. Ecohydrologic separation of water between trees and streams in a Mediterranean climate. Nature Geoscience, 3(2): 100–104.

Brum M, Vadeboncoeur M A, Ivanov V, et al. 2019. Hydrological niche segregation defines forest structure and drought tolerance strategies in a seasonal Amazon forest. Journal of Ecology, 107(1): 318–333.

Brunel J P, Walker G R, Kennett-Smith A K. 1995. Field validation of isotopic procedures for determining sources of water used by plants in a semi-arid environment. Journal of Hydrology, 167(1–4): 351–368.

Chang E, Li P, Li Z, et al. 2019. Using water isotopes to analyze water uptake during vegetation succession on abandoned cropland on the Loess Plateau, China. CATENA, 181: 104095, doi: 10.1016/j.catena.2019.104095.

Chen H, Hu K, Nie Y, et al. 2017. Analysis of soil water movement inside a footslope and a depression in a Karst catchment, Southwest China. Scientific Reports, 7(1): 1–13.

Chen Y, Helliker B R, Tang X, et al. 2020. Stem water cryogenic extraction biases estimation in deuterium isotope composition of plant source water. Proceedings of the National Academy of Sciences of the United States of America, 117(52): 33345–33350.

Chen Z, Wang G, Pan Y, et al. 2021. Water use patterns differed notably with season and slope aspect for *Caragana korshinskii* on the Loess Plateau of China. CATENA, 198: 105028, doi: 10.1016/j.catena.2020.105028.

Chimner R A, Cooper D J. 2004. Using stable oxygen isotopes to quantify the water source used for transpiration by native shrubs in the San Luis Valley, Colorado USA. Plant and Soil, 260(1–2): 225–236.

Craig H. 1961. Isotopic variations in meteoric waters. Science, 133(3465): 1702–1703.

Cui Y Q, Ma J Y, Sun W, et al. 2015. A preliminary study of water use strategy of desert plants in Dunhuang, China. Journal of Arid Land, 7(1): 73–81.

Dai Y, Zheng X J, Tang L S, et al. 2015. Stable oxygen isotopes reveal distinct water use patterns of two *Haloxylon* species in the Gurbantonggut Desert. Plant and Soil, 389(1–2): 73–87.

Dawson T E, Ehleringer J R. 1991. Streamside trees that do not use stream water. Nature, 350(6316): 335–337.

Dawson T E, Pate J S. 1996. Seasonal water uptake and movement in root systems of Australian phraeatophytic plants of dimorphic root morphology: a stable isotope investigation. Oecologia, 107: 13–20.

Duan D Y, Hua Q Y, Song M H, et al. 2008. Water sources of dominant species in three alpine ecosystems on the Tibetan Plateau, China. Journal of Integrative Plant Biology, 50(3): 257–264.

Eggemeyer K D, Awada T, Harvey F E, et al. 2009. Seasonal changes in depth of water uptake for encroaching trees *Juniperus virginiana* and *Pinus ponderosa* and two dominant C_4 grasses in a semiarid grassland. Tree Physiology, 29(2): 157–169.

Ehleringer J R, Dawson T E. 1992. Water uptake by plants: perspectives from stable isotope composition. Plant, Cell and Environment, 15(9): 1073–1082.

Ellsworth P Z, Williams D G. 2007. Hydrogen isotope fractionation during water uptake by woody xerophytes. Plant and Soil, 291(1–2): 93–107.

Evaristo J, Jasechko S, McDonnell J J. 2015. Global separation of plant transpiration from groundwater and streamflow. Nature, 525(7567): 91–94.

Fang X W, Turner N C, Xu D H, et al. 2013. Limits to the height growth of *Caragana korshinskii* resprouts. Tree Physiology, 33(3): 275–284.

Gao X, Wu P, Zhao X, et al. 2011. Soil moisture variability along transects over a well-developed gully in the Loess Plateau, China. CATENA, 87(3): 357–367.

Gao X, Zhao X, Li H, et al. 2018. Exotic shrub species (*Caragana korshinskii*) is more resistant to extreme natural drought than native species (*Artemisia gmelinii*) in a semiarid revegetated ecosystem. Agricultural and Forest Meteorology, 263: 207–216.

Geris J, Tetzlaff D, McDonnell J J, et al. 2017. Spatial and temporal patterns of soil water storage and vegetation water use in humid northern catchments. Science of the Total Environment, 595: 486–493.

Goldsmith G R, Allen S T, Braun S, et al. 2019. Spatial variation in throughfall, soil, and plant water isotopes in a temperate forest. Ecohydrology, 12(2): e2059, doi: 10.1002/eco.2059.

Hannes D D, Hervé-Fernández P, Stahl C, et al. 2018. Liana and tree below-ground water competition-evidence for water resource partitioning during the dry season. Tree Physiology, 38(7): 1071–1083.

Heras M, Espigares T, Merino-Martín L, et al. 2011. Water-related ecological impacts of rill erosion processes in Mediterranean-dry reclaimed slopes. CATENA, 84(3): 114–124.

Huo G, Zhao X, Gao X, et al. 2018. Seasonal water use patterns of rainfed jujube trees in stands of different ages under semiarid plantations in China. Agriculture, Ecosystems and Environment, 265(26): 392–401.

Jia Z, Zhu Y, Liu L. 2012. Different water use strategies of juvenile and adult *Caragana intermedia* plantations in the Gonghe Basin, Tibet Plateau. PLoS ONE, 7(9): e45902, doi: 10.1371/journal.pone.0045902.

Landwehr J M, Coplen T B. 2006. Line-conditioned excess: a new method for characterizing stable hydrogen and oxygen isotope ratios in hydrologic systems. In: International Conference on Isotopes in Environmental Studies. Monte Carlo: International Atomic Energy Agency, 132–135.

Landwehr J M, Coplen T B, Stewart D W. 2014. Spatial, seasonal, and source variability in the stable oxygen and hydrogen isotopic composition of tap waters throughout the USA. Hydrological Processes, 28(21): 5382–5422.

Leen J B, Berman E S F, Liebson L, et al. 2012. Spectral contaminant identifier for off-axis integrated cavity output spectroscopy measurements of liquid water isotopes. Review of Scientific Instruments: 83(4): 044305, doi: 10.1063/1.4704843.

Li C, Guo J H, Zeng F, et al. 2015. Shoot and root architectural variance and adaptability of *Tamarix ramosissimain* different ages. Journal of Desert Research, 35(2): 365–372. (in Chinese)

Li Y, Ma Y, Song X, et al. 2021. A δ^2H offset correction method for quantifying root water uptake of riparian trees. Journal of Hydrology, 593: 125811, doi: 10.1016/j.jhydrol.2020.125811.

Lin G, Sternberg L da S L. 1993. Hydrogen isotopic fractionation by plant roots during water uptake in coastal wetland plants. In: Harold A M. Stable Isotopes and Plant Carbon-water Relations. California: Academic Press, 497–510.

Martín-Gómez P, Serrano L, Ferrio J P. 2017. Short-term dynamics of evaporative enrichment of xylem water in woody stems: Implications for ecohydrology. Tree Physiology, 37(4): 511–522.

Moreno-Gutiérrez C, Dawson T E, Nicolás E, et al. 2012. Isotopes reveal contrasting water use strategies among coexisting plant species in a mediterranean ecosystem. New Phytologist, 196(2): 489–496.

Nie Y P, Chen H S, Wang K L, et al. 2011. Seasonal water use patterns of woody species growing on the continuous dolostone outcrops and nearby thin soils in subtropical China. Plant and Soil, 341(1–2): 399–412.

Oerter E J, Siebert G, Bowling D R, et al. 2019. Soil water vapour isotopes identify missing water source for streamside trees. Ecohydrology, 12(4): e2083, doi: 10.1002/eco.2083.

Ogle K, Reynolds J F. 2004. Plant responses to precipitation in desert ecosystems: Integrating functional types, pulses,

thresholds, and delays. Oecologia, 141(2): 282–294.

Porporato A, Daly E, Rodriguez-Iturbe I. 2004. Soil water balance and ecosystem response to climate change. The American Naturalist, 164(5): 625.

Rossatto D R, de Carvalho Ramos Silva L, Villalobos-Vega R, et al. 2012. Depth of water uptake in woody plants relates to groundwater level and vegetation structure along a topographic gradient in a neotropical savanna. Environmental and Experimental Botany, 77: 259–266.

Rothfuss Y, Javaux M. 2017. Reviews and syntheses: Isotopic approaches to quantify root water uptake: A review and comparison of methods. Biogeosciences, 14(8): 2199–2224.

Schenk H J. 2008. Soil depth, plant rooting strategies and species' niches. New Phytologist, 178(2): 223–225.

Schultz N M, Griffis T J, Lee X, et al. 2011. Identification and correction of spectral contamination in $^{2}H/^{1}H$ and $^{18}O/^{16}O$ measured in leaf, stem, and soil water. Rapid Communications in Mass Spectrometry, 25(21): 3360–3368.

Sprenger M, Leistert H, Gimbel K, et al. 2016. Illuminating hydrological processes at the soil-vegetation-atmosphere interface with water stable isotopes. Reviews of Geophysics, 54(3): 674–704.

Sprenger M, Tetzlaff D, Soulsby C. 2017. Soil water stable isotopes reveal evaporation dynamics at the soil-plant-atmosphere interface of the critical zone. Hydrology and Earth System Sciences, 21(7): 3839–3856.

Stock B C, Semmens B X. 2013. MixSIAR GUI User Manual. Version 3.1, 1–42. [2021-10-11]. https://doi.org/10.5281/zenodo.47719.1.

Su P Y, Zhang M J, Qu D Y, et al. 2020. Contrasting water use strategies of *Tamarix ramosissima* in different habitats in the northwest of loess plateau, China. Water, 12(10): 2791.

Sun S J, Meng P, Zhang J S, et al. 2011. Variation in soil water uptake and its effect on plant water status in J*uglans regia* L. during dry and wet seasons. Tree Physiology, 31(12): 1378–1389.

Vargas A I, Schaffer B, Li Y H, et al. 2017. Testing plant use of mobile vs immobile soil water sources using stable isotope experiments. New Phytologist, 215(2): 582–594.

Wang J, Fu B J, Lu N, et al. 2017. Seasonal variation in water uptake patterns of three plant species based on stable isotopes in the semi-arid Loess Plateau. Science of the Total Environment, 609: 27–37.

Wang J, Lu N, Fu B J. 2019. Inter-comparison of stable isotope mixing models for determining plant water source partitioning. Science of the Total Environment, 666: 685–693.

Williams D G, Ehleringer J R. 2000. Intra- and inter-specific variation for summer precipitation use in pinyon-juniper woodlands. Ecological Monographs, 70(4): 517–537.

Wu L, Su S, Wang H. 2006. Preliminary investigation into plant and vegetation types in afforestation region in southern and northern mountains of Lanzhou City. Journal of Desert Research, 26(4): 564–568. (in Chinese)

Yang B, Wen X, Sun X. 2015. Seasonal variations in depth of water uptake for a subtropical coniferous plantation subjected to drought in an East Asian monsoon region. Agricultural and Forest Meteorology, 201: 218–228.

Yang L, Wei W, Chen L, et al. 2014. Response of temporal variation of soil moisture to vegetation restoration in semi-arid Loess Plateau, China. CATENA, 115: 123–133.

Yao J, Chen Y, Zhao Y, et al. 2020. Climatic and associated atmospheric water cycle changes over the Xinjiang, China. Journal of Hydrology, 585: 124823, doi: 10.1016/j.jhydrol.2020.124823.

Zhang Q, Yang J, Wang W, et al. 2021. Climatic warming and humidification in the arid region of Northwest China: multi-scale characteristics and impacts on ecological vegetation. Journal of Meteorological Research, 35(1): 113–127.

Zhang Y, Zhang M J, Qu D Y, et al. 2020. Water use strategies of dominant species (*Caragana korshinskii* and *Reaumuria soongorica*) in natural shrubs based on stable isotopes in the Loess Hill, China. Water, 12(7): 1923.

Zhou H, Zhao W, He Z. 2017. Water sources of *Nitraria sibirica* and response to precipitation in two desert habitats. Chinese Journal of Applied Ecology, 28(7): 2083–2092. (in Chinese)

Appendix

Table S1 Isotopic composition of different types of water body

Sample		δ^2H (‰)			$\delta^{18}O$ (‰)		
		Min	Max	Mean	Min	Max	Mean
Precipitation		–126.82	–28.73	–49.91*	–18.06	1.58	–8.21*
Soil water	Juvenile *C. korshinskii*	–82.43	–24.28	–50.48	–12.88	5.07	–4.69
	Intermediate *C. korshinskii*	–86.68	–6.93	–48.77	–13.34	7.76	–5.27
	Adult *C. korshinskii*	–87.52	–22.63	–56.60	–14.53	4.18	–7.01
	Juvenile *T. ramosissima*	–80.11	0.63	–46.60	–12.26	10.34	–4.27
	Intermediate *T. ramosissima*	–76.72	–10.00	–43.73	–11.96	12.45	–1.06
	Adult *T. ramosissima*	–80.36	–9.70	–39.03	–12.35	9.85	–0.38
Plant xylem water	Juvenile *C. korshinskii*	–71.40	–27.33	–47.89	–8.64	0.22	–3.83
	Intermediate *C. korshinskii*	–63.97	–27.04	–45.48	–7.67	–2.34	–4.55
	Adult *C. korshinskii*	–58.48	–33.58	–47.17	–7.30	–2.44	–5.27
	Juvenile *T. ramosissima*	–69.87	–49.46	–62.16	–9.80	–6.00	–7.64
	Intermediate *T. ramosissima*	–70.12	–48.69	–57.84	–9.83	–4.94	–6.81
	Adult *T. ramosissima*	–70.25	–19.40	–56.61	–9.78	1.50	6.60

Note: * represent annual weighted mean precipitation. Min, minimum; Max, maximum.

Table S2 Contributions of three modes of data input to the MixSIAR model

Input data mode	Contributions (%)							
	0–10 cm		10–40 cm		40–100 cm		100–200 cm	
	Mean	SD	Mean	SD	Mean	SD	Mean	SD
δ^2H and $\delta^{18}O$	29.67	12.71	22.72	14.33	22.22	12.12	25.38	14.76
$\delta^2H_{\_c1}$ and $\delta^{18}O$	28.80	12.01	20.78	15.04	23.11	12.47	27.31	14.34
$\delta^2H_{\_c2}$ and $\delta^{18}O$	26.80	12.07	25.31	14.67	20.65	11.7	27.23	15.00

Note: SD, standard deviation.

Table S3 Contribution of the 0–40 cm soil water for *C. korshinskii* at different ages after rainfall

Plant	Date	Contribution of the 0–40 cm soil water (%)		
		δ^2H and $\delta^{18}O$	$\delta^2H_{\_c1}$ and $\delta^{18}O$	$\delta^2H_{\_c2}$ and $\delta^{18}O$
Juvenile *C. korshinskii*	19 Jul (1 d after rainfall)	79.8	49.6	86.0
	21 Jul (3 d after rainfall)	51.6	46.4	47.8
	23 Jul (5 d after rainfall)	54.5	50.0	43.3
Intermediate *C. korshinskii*	19 Jul (1 d after rainfall)	83.7	83.4	86.8
	21 Jul (3 d after rainfall)	71.3	45.2	91.6
	23 Jul (5 d after rainfall)	54.2	48.2	62.9
Adult *C. korshinskii*	19 Jul (1 d after rainfall)	53.8	23.7	87.9
	21 Jul (3 d after rainfall)	32.0	33.9	23.2
	23 Jul (5 d after rainfall)	58.1	60.0	50.1
Juvenile *C. korshinskii*	24 Aug (1 d after rainfall)	11.1	10.8	8.2
	26 Aug (3 d after rainfall)	93.6	91.0	86.8
	28 Aug (5 d after rainfall)	94.0	93.6	89.5
Intermediate *C. korshinskii*	24 Aug (1 d after rainfall)	61.6	61.1	85.2
	26 Aug (3 d after rainfall)	78.8	52.4	54.4
	28 Aug (5 d after rainfall)	87.6	81.9	72.6
Adult *C. korshinskii*	24 Aug (1 d after rainfall)	55.8	49.1	54.2
	26 Aug (3 d after rainfall)	22.9	21.8	17.7
	28 Aug (5 d after rainfall)	31.6	30.4	19.5

Table S4 Contribution of the 0–40 cm soil water for *T. ramosissim* at different ages after rainfall

Plant	Date	Contribution of the 0–40 cm soil water (%)		
		δ^2H and $\delta^{18}O$	$\delta^2H_{\_c1}$ and $\delta^{18}O$	$\delta^2H_{\_c2}$ and $\delta^{18}O$
Juvenile *T. ramosissim*	19 Jul (1 d after rainfall)	77.6	58.9	54.0
	21 Jul (3 d after rainfall)	21.2	27.3	7.8
	23 Jul (5 d after rainfall)	21.0	17.5	34.4
Intermediate *T. ramosissim*	19 Jul (1 d after rainfall)	95.3	93.6	2.9
	21 Jul (3 d after rainfall)	53.8	72.1	35.0
	23 Jul (5 d after rainfall)	46.6	42.9	24.6
Adult *T. ramosissim*	19 Jul (1 d after rainfall)	90.1	89.0	89.0
	21 Jul (3 d after rainfall)	99.1	99.0	99.0
	23 Jul (5 d after rainfall)	27.7	22.3	35.9
Juvenile *T. ramosissim*	24 Aug (1 d after rainfall)	55.3	47.3	45.6
	26 Aug (3 d after rainfall)	97.1	94.7	94.1
	28 Aug (5 d after rainfall)	66.4	99.6	99.4
Intermediate *T. ramosissim*	24 Aug (1 d after rainfall)	60.9	67.5	43.5
	26 Aug (3 d after rainfall)	35.8	39.7	65.3
	28 Aug (5 d after rainfall)	82.3	81.2	79.7
Adult *T. ramosissim*	24 Aug (1 d after rainfall)	79.1	74.1	73.2
	26 Aug (3 d after rainfall)	93.7	93.1	91.5
	28 Aug (5 d after rainfall)	8.4	12.0	12.1

Table S5 Correlation between contribution calculated by $\delta^2H_{\_c2}$ and $\delta^{18}O$ input into the MixSIAR model and cumulative rainfall amount of 7 d before sampling

Plant	Depth (cm)	Rainfall (7 d amount)	VPD (7d mean)	0–10 cm SWC	10–40 cm SWC	40–100 cm SWC	100–200 cm SWC
Juvenile *C. korshinskii*	0–10	–0.365	0.174	–0.375	0.177	–0.039	–0.014
	10–40	–0.118	–0.072	–0.095	–0.686*	–0.488	–0.416
	40–100	–0.081	0.008	–0.345	–0.615	–0.412	–0.382
	100–200	0.639	–0.211	0.826**	0.579	0.626	0.530
Intermediate *C. korshinskii*	0–10	0.332	–0.602	–0.244	–0.342	–0.387	–0.335
	10–40	–0.234	0.210	0.795**	0.659*	–0.618	0.587
	40–100	–0.242	0.398	–0.067	0.066	–0.068	–0.007
	100–200	–0.032	0.351	–0.636*	–0.405	–0.217	–0.284
Adult *C. korshinskii*	0–10	0.019	–0.198	–0.090	0.035	0.228	0.333
	10–40	–0.286	–0.106	–0.284	–0.148	0.039	–0.140
	40–100	–0.169	0.258	0.460	0.316	–0.013	–0.345
	100–200	0.255	–0.046	–0.213	–0.250	–0.197	0.113
Juvenile *T. ramosissim*	0–10	0.183	0.251	0.405	0.414	0.231	0.161
	10–40	0.153	–0.610	–0.046	–0.078	–0.316	–0.412
	40–100	0.475	–0.047	–0.410	–0.427	–0.357	–0.174
	100–200	–0.688*	0.199	0.008	0.034	0.294	0.263
Intermediate *T. ramosissim*	0–10	0.117	0.288	–0.027	0.343	0.669*	0.718*
	10–40	0.598	–0.440	0.049	–0.306	–0.588	–0.580
	40–100	–0.876**	–0.250	0.688*	0.685*	0.156	0.174
	100–200	–0.083	0.246	–0.370	–0.421	–0.214	–0.298
Adult *T. ramosissim*	0–10	0.110	0.799*	0.579	0.454	0.383	0.366
	10–40	–0.712*	–0.263	0.339	0.321	0.255	0.514
	40–100	0.626	–0.603	–0.589	–0.500	–0.349	–0.584
	100–200	–0.773	–0.295	–0.109	–0.046	–0.151	0.151

Note: VPD, vapour pressure deficit; SWC, soil water content; *, $P<0.05$ level; **, $P<0.05$ level.

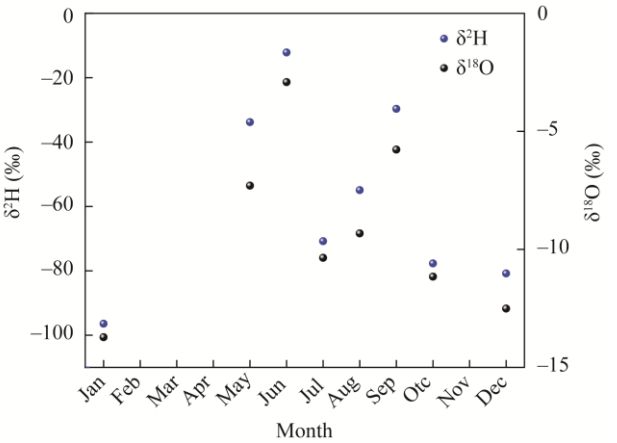

Fig. S1 Variation of monthly precipitation weighted δ^2H and $\delta^{18}O$. No precipitation data in February, March, April, and November.

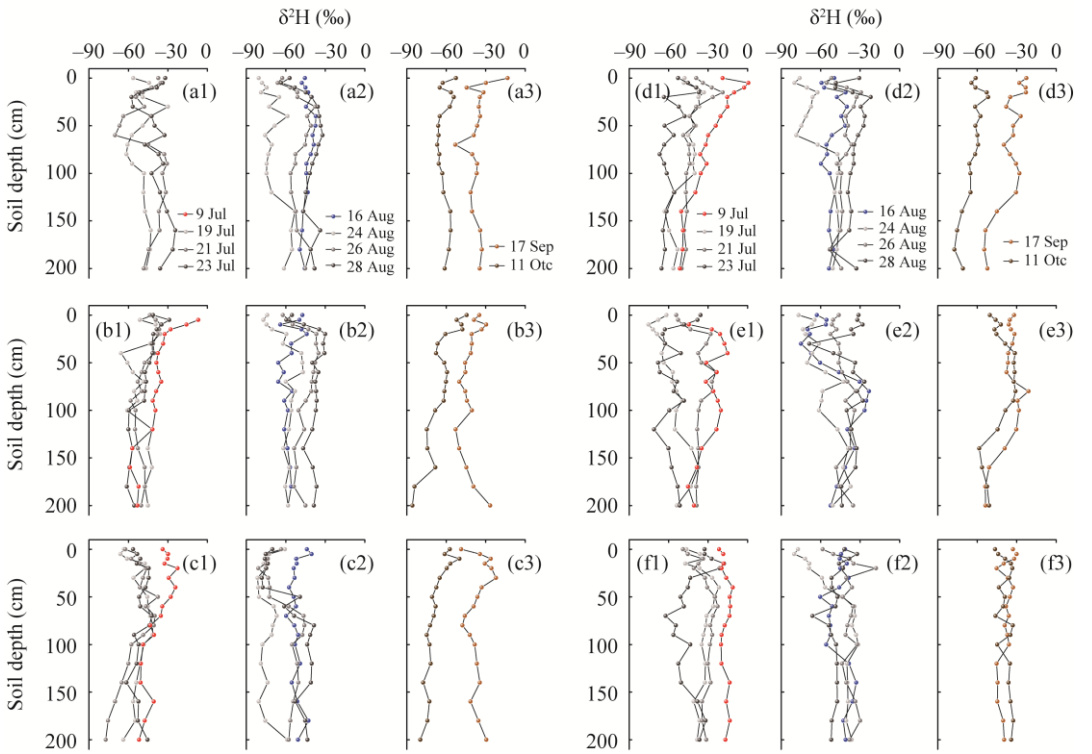

Fig. S2 Variation of soil water δ^2H in juvenile *C. korshinskii* (a1–a3), intermediate *C. korshinskii* (b1–b3), adult *C. korshinskii* (c1–c3), and juvenile *T. ramosissima* (d1–d3), intermediate *T. ramosissima* (e1–e3), and adult *T. ramosissima* (f1–f3)

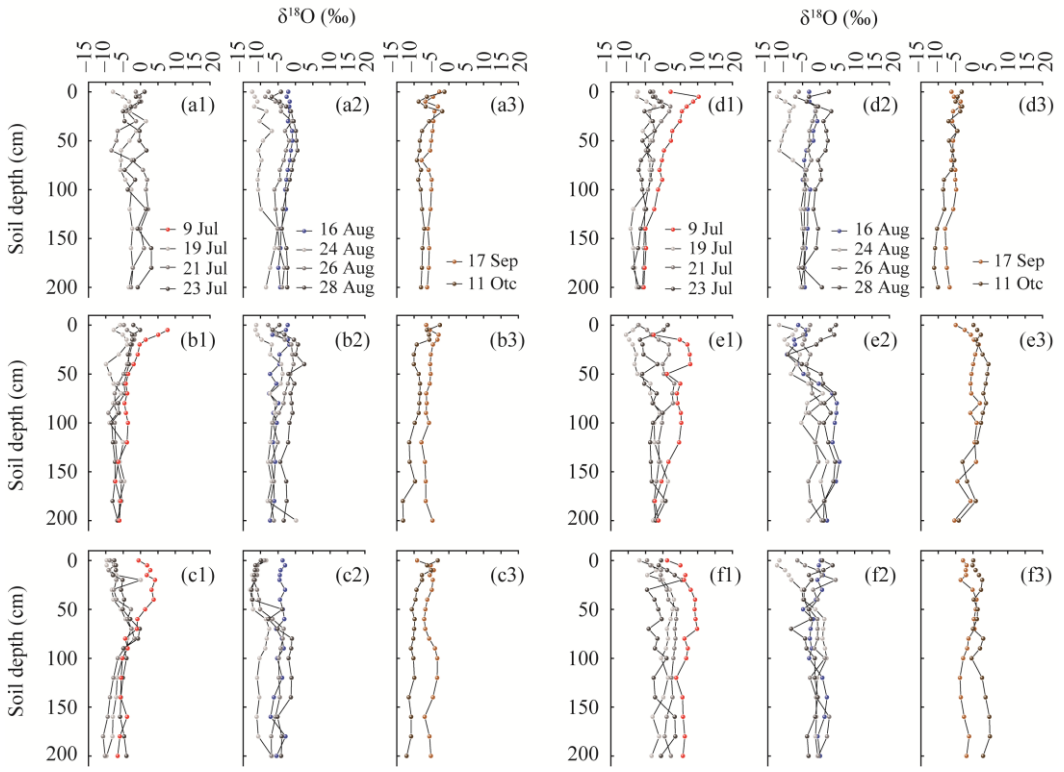

Fig. S3 Variation of soil water $\delta^{18}O$ in juvenile *C. korshinskii* (a1–a3), intermediate *C. korshinskii* (b1–b3), adult *C. korshinskii* (c1–c3), juvenile *T. ramosissima* (d1–d3), intermediate *T. ramosissima* (e1–e3), and adult *T. ramosissima* (f1–f3)

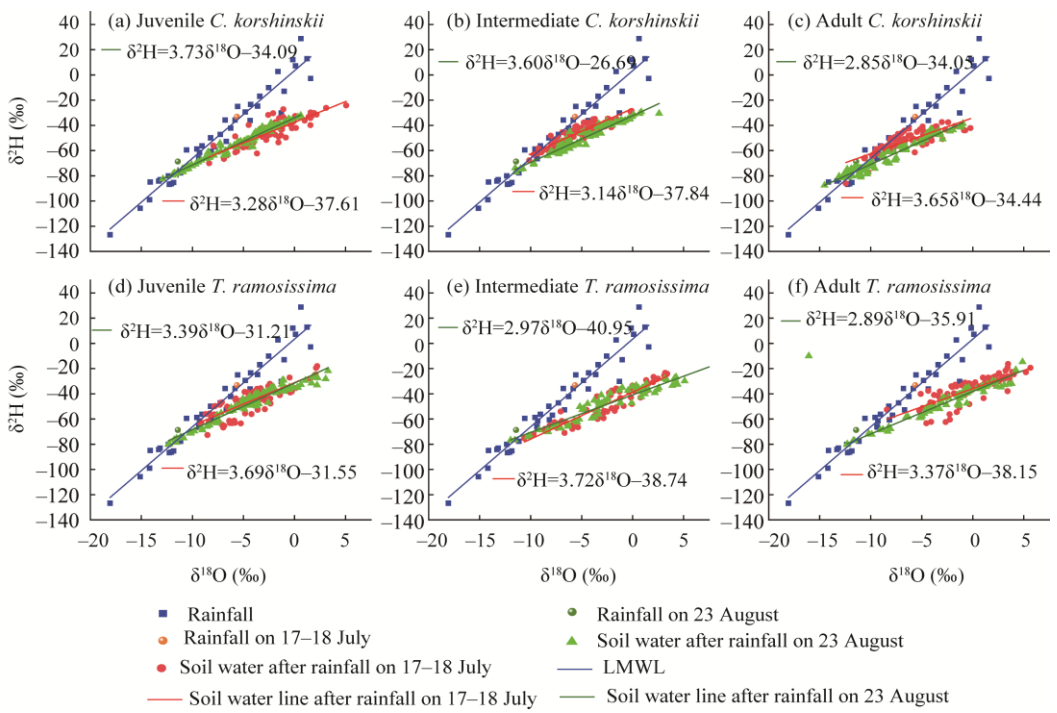

Fig. S4 Linear regression relationship between $\delta^{2}H$ and $\delta^{18}O$ in soil water after rainfall on 17–18 July and 23 August in juvenile, intermediate, and adult *C. korshinskii* (a–c), and juvenile, intermediate, and adult *T. ramosissima* (d–f). LMWL is the local meteoric water line.